Current-Sensorless Robust Sliding Mode Control for the Interleaved DC-DC Boost Converter

Said Oucheriah (soucheria@niu.edu).
Department of Engineering Technology Northern Illinois University, Illinois, USA.
.

***Abstract*—A current-sensorless, PWM-based robust sliding mode control strategy for the interleaved DC-DC boost converter is proposed, requiring only output-voltage measurement. An extended state estimator is developed to estimate the derivative of the output voltage alongside a lumped uncertainty term that comprises inductor parasitic resistance, component parameter uncertainties, load and input voltage variations. A linear sliding surface is then utilized to derive a controller that features a simple design yet exhibits excellent robustness against external disturbances, parameter variations, and parasitics, despite the absence of inductor current feedback. Additionally, a systematic step-by-step procedure to select the controller and estimator gains is outlined. The tracking performance and robust capabilities of the proposed control system are validated through comprehensive computer simulations.**

Keywords: Robust sliding mode control, interleaved DC-DC boost converter, current-sensorless control, extended state estimator.

I. Introduction

DC-DC converters are subjected to external disturbances, parameter uncertainties, and parasitics that must be taken into account in the design of robust controllers to tightly track the output reference voltage and seek a reduction in the number of sensors needed for their implementation. PWM-sliding mode control (SMC) in conjunction with disturbance estimators is a powerful nonlinear control strategy that can be used. However, in many cases, the designed controllers require knowledge of the inductor current. Its measurement can present challenges in the presence of external disturbances and high-frequency noise that can be amplified, leading to chattering in the control signal. This has led to the use of current sensor-free controllers, which offer a reduction in cost and an improvement in the reliability and miniaturization of the device.

In the context of DC-DC boost converters [1-7], the design of robust current sensor-free controllers is a challenging task since the boost converter is a nonminimum phase system. While many of these approaches effectively address the issue of output voltage regulation of DC-DC boost converters, they often have limitations. Some control laws proposed are complicated and computationally intensive to render them impractical in real applications. They may also involve many design parameters that require very laborious parameter tuning, with some lacking rigorous stability analysis of the closed-loop systems. Lastly, with few exceptions, robustness tests to parameter uncertainties and parasitics of the converter are not analyzed and ignored in simulations and may lead to substantial steady-state errors in the output response. To address these problems, an extended state estimator is developed in [8], to estimate a lumped uncertainty that comprises the uncertain load and input voltage, the converter parasitics and the component uncertainties and estimate the derivative of the output voltage. The salient feature of the controller is its very simple design and its robustness to external disturbances and parameter uncertainties despite the absence of the inductor current feedback. In addition, a very simple procedure to select the controller/estimator gains is outlined.

Recently, there is a great interest in interleaved boost converter (IBC) topology, which is being rapidly adopted in renewable energy systems, electric vehicles, and battery charging systems. They are characterized by multiple parallel-connected boost converter stages and offer many advantages over the classical boost converter. These are a reduction in thermal and electrical component stress due to current-sharing capability, an increase in efficiency and power handling capability and a reduction in passive component sizes as compared to the traditional single phase converter.

In [9], a nonlinear disturbance observer (NDO)-based sliding-mode control algorithm is proposed to estimate two lumped disturbances whose derivatives in the limit are assumed zero. The implementation requires the output voltage, the input current and input voltage measurements. In [10], a super-twisting sliding mode control law is proposed for interleaved dc-dc boost converter for fuel cell application based on the double-loop control structure containing two inductor current inner-loops and an output voltage outer-loop. An extended-state-observer (ESO) is used to estimate the total disturbance that comprises the unknown load power and parametric variations. The implementation of the controller requires an inductor current sensor for each phase and the measurements of the input and output voltages. In [11], a robust model predictive control is proposed to regulate the output voltage of a DC-DC floating interleaved boost converter (FIBC) in the presence of parametric uncertainties. The controller is also able to handle input-output constraints. The proposed control algorithm requires extensive computations solving online min-max optimization problems which makes it of little practical interest and unsuitable for systems with low processing capabilities. Also, it needs a sensor to measure the inductor current.

The study in [12] considers an interleaved DC/DC boost converter supplying a DC-bus with generally unknown loads connected to it. An observer based adaptive controller using the immersion and invariance observer with an energy shaping plus damping injection passivity based controller is proposed. However, the controller requires the measurement of each leg current inductor to ensure equal leg currents. In [13], a controller that is composed of an inner voltage PI loop and an outer voltage PI loop is proposed for the interleaved boost converter. The implementation of the controller requires one input current sensor and one voltage sensor.

In [14] and [17] a robust sliding mode nonlinear controller is designed for an interleaved boost converter based on an extended linearization and active compensation of the lumped disturbance estimated by a linear extended state observer. Simulation and experimental results show that the proposed controller is robust against parameter uncertainties and external disturbances. However, an input current sensor is required for the implementation of the controller.

In [15], a nonlinear fast terminal sliding mode control and a state and disturbance estimation algorithm to estimate the inductor current and a lumped disturbance that includes the load resistance for a two-phase interleaved boost converter is proposed. The stability of the observer is analyzed using Kharitonovs stability criteria. However, the implementation of the controller requires the measurement of the input voltage. In [16], an integral sliding mode controller for the control of a 2PIBC converter is proposed. A lumped disturbance that comprises parameter uncertainties, input voltage and load resistance is estimated using a disturbance observer. The implementation of the controller requires the measurement of the input current.

In this work, there is no need to measure the line and inductor currents. Instead, the derivative of the output voltage is estimated and used in the controller feedback. An extended state estimator is developed to estimate a lumped disturbance signal that includes parameter uncertainties, load and input variations, inductor parasitics and to estimate the derivative of the output voltage. A linear sliding surface is used to derive the controller. A salient feature of this work is the simplicity of the design of the controller with a very simple procedure to select the parameters of the sliding mode controller. The proposed controller is capable of dynamically compensating for the disturbance to achieve a high performance in terms of disturbance rejection despite the absence of the inductor current feedback. The robustness of the proposed controller is validated using simulations.

II. Robust sliding mode control design

A. Two-phase interleaved boost converter averaged model

A basic two-phase interleaved boost converter averaged model is shown in Figure 1. Under continuous conduction mode, the averaged model is:

$$
\begin{aligned}
\dot{i}_{L_1} &= -\frac{R_{L_1}}{L_1} i_{L_1} - (1-u)\frac{v_c}{L_1} + \frac{E}{L_1} \\
\dot{i}_{L_2} &= -\frac{R_{L_2}}{L_2} i_{L_2} - (1-u)\frac{v_c}{L_2} + \frac{E}{L_2} \\
\dot{v}_c &= (1-u)\frac{i_{L_1}}{C} + (1-u)\frac{i_{L_2}}{C} - \frac{v_c}{RC}
\end{aligned}
\tag{1}
$$

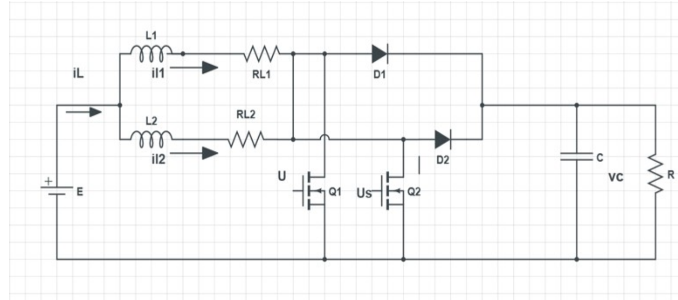

Fig. 1. Circuit diagram of the two-phase interleaved boost converter.

where i_{L_1} and i_{L_2} represent the average inductor currents through inductors L_1 and L_2, respectively, v_c is the output voltage across the capacitor C. The unknown parameters E and R represent the input voltage and the load resistance, respectively. However, their respective nominal values E_o and R_o are assumed known for the implementation of the controller. The control input u to the converter is the duty ratio function and u_s is the same duty ratio as u but staggered in phase by an angle of 180^o.

The symmetrical circuit parameters are in general considered for the design of the controller and therefore we assume $L_1 = L_2 = L$ and $R_{L_1} = R_{L_2} = R_L$. This yields the equivalent mono-phase boost converter model described by the following equations:

$$
\begin{aligned}
\dot{i}_L &= -\frac{R_L}{L} i_L - 2(1-u)\frac{v_c}{L} + \frac{2E}{L} \\
\dot{v}_c &= (1-u)\frac{i_L}{C} - \frac{v_c}{RC}
\end{aligned}
\tag{2}
$$

where $i_L = i_{L_1} + i_{L_2}$.

Taking the derivative of both sides of the second equation of (2) and using the expression for $\dot{i}_L$ given by the first equation of (2) yields

$$
\ddot{v}_c = \frac{u}{L_o C_o}[4v_c - 2E_o] + d \tag{3}
$$

where

$$
\begin{aligned}
d = &-\frac{2v_c}{LC}(1+u^2) + \frac{2E}{LC} - \frac{R_L}{LC}(1-u)i_L \\
&-\dot{u}\frac{i_L}{C} - u\frac{(4v_c - 2E_o)}{L_o C_o} + u\frac{(4v_c - 2E)}{LC} - \frac{1}{RC}\dot{v}_c
\end{aligned}
\tag{4}
$$

In addition to the inductor parasitic, other parasitics such as the MOSFET on-resistance, the diode forward resistance, the conducting voltage of the diode and the capacitor equivalent series resistance could have easily been lumped in the disturbance signal $d(t)$.

Let

$$
\begin{aligned}
e_2 &= v_c - V_{ref} \\
e_1 &= \dot{e}_2
\end{aligned}
\tag{5}
$$

Using the substitution $v_c = e_2 + V_{ref}$ and $\ddot{v}_c = \dot{e}_1$ into (3) yields

$$\begin{aligned} \dot{e}_1 &= \frac{u}{L_o C_o}\Big[4(e_2+V_{ref})-2E_o\Big]+d \\ \dot{e}_2 &= e_1 \end{aligned} \tag{6}$$

B. Design of the extended state estimator

By using the lumped uncertainty d given by (4) as a state variable, the extended state estimator for the system (6) is

$$\begin{aligned} \dot{q}_1 &= \frac{u}{L_o C_o}\Big[4(e_2+V_{ref})-2E_o\Big] \\ &\quad + q_3 + K_3 e_2 - K_1 q_1 - K_1^2 e_2 \\ \dot{q}_2 &= q_1 + K_1 e_2 + K_2 \tilde{q}_2 \\ \dot{q}_3 &= -K_3 q_1 - K_1 K_3 e_2 \end{aligned} \tag{7}$$

The states $\hat{e}_1,\ \hat{e}_2$ and $\hat{d}$ are the estimates of e_1, e_2 and d respectively and are given by:

$$\hat{e}_1 = q_1 + K_1 e_2,\ \hat{e}_2 = q_2,\ \hat{d} = q_3 + K_3 e_2 \tag{8}$$

with $\tilde{q}_2 = e_2 - \hat{e}_2$. The parameters K_1, K_2 and K_3 are the estimator gains. Using (6), (7) and (8), the dynamics of the state errors are

$$\begin{aligned} \dot{\tilde{e}}_1 &= -K_1\tilde{e}_1 + \tilde{d} \\ \dot{\tilde{e}}_2 &= \tilde{e}_1 - K_2\tilde{e}_2 \\ \dot{\tilde{d}} &= -K_3\tilde{e}_1 + \dot{d} \end{aligned} \tag{9}$$

with $\tilde{e}_1 = e_1 - \hat{e}_1,\ \tilde{e}_2 = e_2 - \hat{e}_2$ and $\tilde{d} = d - \hat{d}$. System (9) can be written in compact form as

$$\dot{\tilde{e}} = A\tilde{e} + B\dot{d} \tag{10}$$

where $\tilde{e} = [\tilde{e}_1,\ \tilde{e}_2,\ \tilde{d}]^T$ and

$$A = \begin{bmatrix} -K_1 & 0 & 1 \\ 1 & -K_2 & 0 \\ -K_3 & 0 & 0 \end{bmatrix},\ B = \begin{bmatrix} 0 \\ 0 \\ 1 \end{bmatrix} \tag{11}$$

Assumption 1: We assume that for any bounded time-varying lumped disturbance d we have

$$\delta = \sup_{t\in[0\ \infty)} \|\dot{d}\| \tag{12}$$

The eigenvalues of the system matrix A are determined from the characteristic equation

$$\begin{aligned} s^3 + (K_1+K_2)\,s^2 + \big(K_1K_2 + K_3\big)\,s \\ + K_2K_3 = 0 \end{aligned} \tag{13}$$

For any $K_1 > 0, K_2 > 0$ and $K_3 > 0$, the poles are on the left-half side of the complex plane with the matrix A being Hurwitz.

If

$$2\sqrt{K_3} < K_1 \tag{14}$$

then the time-invariant system (10) is overdamped with three real distinct and negative poles.

If

$$2\sqrt{K_3} = K_1 \tag{15}$$

then the time-invariant system (10) is operating under a critically damped regime. A third order system with a dominant critically second-order dominant subsystem with negative repeated poles.

In both cases, the state errors are strictly and tightly bounded by

$$\limsup_{t\to\infty} |\tilde{e}_1(t)| \le \frac{\delta}{K_3}\cdot \tag{16}$$

$$\limsup_{t\to\infty} |\tilde{e}_2(t)| \le \frac{\delta}{K_2K_3}\cdot \tag{17}$$

$$\limsup_{t\to\infty} |\tilde{d}(t)| \le \frac{\delta K_1}{K_3}\cdot \tag{18}$$

For the case

$$2\sqrt{K_3} > K_1 \tag{19}$$

The time-invariant system is operating under an underdamped regime, a third order system with a dominant underdamped second order subsystem. In this case the state errors are strictly and tightly bounded by

$$\limsup_{t\to\infty} |\tilde{e}_1(t)| \le \frac{\delta}{K_3}\cdot A_{\max} \tag{20}$$

$$\limsup_{t\to\infty} |\tilde{e}_2(t)| \le \frac{\delta}{K_2K_3}\cdot A_{\max} \tag{21}$$

$$\limsup_{t\to\infty} |\tilde{d}(t)| \le \frac{\delta K_1}{K_3}\cdot A_{\max} \tag{22}$$

where $A_{\max}$ is a unified global resonance amplification multiplier and a function of the system's internal damping ratio.

Remark 1: If $\lim_{t\to\infty}\dot{d}(t) = 0$, then all states will asymptotically decay to zero as time goes to infinity and we have

$$\lim_{t\to\infty}\tilde{e}_1 = 0,\ \lim_{t\to\infty}\tilde{e}_2 = 0,\ \lim_{t\to\infty}\tilde{d} = 0 \tag{23}$$

Since K_3 is typically a very high gain, the steady-state errors of the extended state estimator are usually small and approach uniformly 0 in $t \in [0\ \infty)$ as $K_3 \to \infty$.

C. Design of the controller and stability analysis

We consider the following sliding surface

$$\begin{aligned} \sigma &= \hat{e}_1 + \gamma\hat{e}_2 - K_1 e_2 \\ &= q_1 + \gamma q_2 \end{aligned} \tag{24}$$

where we have used $\hat{e}_1 = q_1 + K_1 e_2$ and $q_2 = \hat{e}_2$ and $\gamma > 0$ is a design parameter. We consider the following controller

$$\begin{aligned} u &= \alpha\,(K_1-\gamma)\,q_1 - \alpha q_3 \\ &\quad + \alpha\,\big(-K_3 + K_1^2 - \gamma K_1\big)\,e_2 - \alpha K_2\gamma\tilde{q}_2 - \alpha K_4\sigma \end{aligned} \tag{25}$$

where

$$\alpha = \frac{L_o C_o}{[4(e_2+V_{ref})-2E_o]} \tag{26}$$

Using (24), the controller (25) is derived by differentiating σ with respect to time and setting $\dot{\sigma} = 0$. The last term $\alpha K_4\sigma$ is added to ensure the sliding mode condition.

The substitution of the controller u into the derivative of (24) leads to

$$\dot{\sigma} = -K_4\sigma \tag{27}$$

and therefore, we have $\dot{\sigma}\sigma = -K_4\sigma^2 < 0$ which ensures the sliding mode condition. Equation (27) admits as a solution

$$\sigma(t) = \sigma(0)e^{-K_4 t} \tag{28}$$

Using the initial conditions $q_1(0) = 0,\ q_2(0) = 0$ for the extended state estimator (7), yields $\sigma(0) = 0$ and in this case $\sigma(t) = 0$ for all $t \geq 0$ with the reaching phase completely eliminated.

Theorem 1: For the system (2) with the extended state estimator (7) and driven by the controller (25), the output voltage $v_c(t)$ is uniformly convergent to a ball $\Omega(r)$ centered at V_{ref} with a radius r given by

$$r = \frac{1}{K_3}\left[1 + \frac{\gamma}{K_2}\right]\frac{\delta}{(\gamma - K_1)} \tag{29}$$

with a decay rate $(\gamma - K_1)$. Here $\gamma > K_1$ with the parameter δ defined in (12).

Proof: Substituting $(e_1 - \tilde{e}_1)$ for $\hat{e}_1,\ (e_2 - \tilde{e}_2)$ for $\hat{e}_2$ and $\sigma = 0$ in equation (24) and solving for e_1 yields

$$e_1 = -(\gamma - K_1)e_2 + \tilde{e}_1 + \gamma\tilde{e}_2 \tag{30}$$

Using $e_1 = \dot{v}_c$ and $e_2 = v_c - V_{ref}$ into (30) yields the following dynamic equation

$$\dot{v}_c = -(\gamma - K_1)(v_c - V_{ref}) + \tilde{e}_1 + \gamma\tilde{e}_2 \tag{31}$$

In this work, we consider condition (15) that yields an extended state estimator operating under a critically damped regime to avoid oscillatory behavior. In this case, the bounds for $\|\tilde{e}_1\|$ and $\|\tilde{e}_2\|$ are given by (16) and (17), respectively. For the underdamped regime case, the bounds (20) and (21) should be used. The solution $v_c(t)$ of (31) is bounded by

$$\begin{gathered}\|v_c(t)\| \leq \\ \left[\|v_c(0)\| - V_{ref} + \frac{1}{K_3}\left[1 + \frac{\gamma}{K_2}\frac{\delta}{(\gamma - K_1)}\right]e^{-(\gamma - K_1)t}\right. \\ \left. + \left[V_{ref} + \frac{1}{K_3}\left[1 + \frac{\gamma}{K_2}\right]\frac{\delta}{(\gamma - K_1)}\right]\right.\end{gathered} \tag{32}$$

and consequently, v_c is uniformly convergent to a ball centered at V_{ref} with a radius r given by (29) and a decay rate $(\gamma - K_1)$.

Remark 2: In the case of step load resistance and step input voltage changes, we may have $\lim_{t\to\infty}\dot{d}(t) = 0$. In this case $v_c(t) \to V_{ref}$. From (3) with $\ddot{v}_c \to 0$ we have

$$u^* = -\alpha_o d^* \tag{33}$$

where $u^* = \lim_{t\to\infty}\dot{u}(t)$, $d^* = \lim_{t\to\infty}d(t)$ and $\alpha_o = \frac{L_oC_o}{\left[4V_{ref} - 2E_o\right]}$.

Using (4) we have

$$\begin{aligned} d^* &= -\frac{2V_{ref}}{LC}(1 + u^{*2}) + \frac{2E}{LC} - \frac{R_L}{LC}(1 - u^*)i_L^* \\ &\quad -u^*\frac{(4V_{ref} - 2E_o)}{L_oC_o} + u^*\frac{(4V_{ref} - 2E)}{LC} \\ d &= -\frac{2V_{ref}}{LC}(1 + u^{*2}) + \frac{2E}{LC} - \frac{R_L}{LC}\frac{V_{ref}}{R} \\ &\quad -u^*\frac{(4V_{ref} - 2E_o)}{L_oC_o} + u^*\frac{(4V_{ref} - 2E)}{LC}\end{aligned} \tag{34}$$

where we have used

$$(1 - u^*)i_L^* = \frac{V_{ref}}{R} \tag{35}$$

which is derived from the second equation of (2) with $\dot{v}_c \to 0$ and we also have used $\dot{u} \to 0$.

The steady state of the controller given in equation (33) is

$$\begin{aligned} u^* = -\alpha_o d^* &= \frac{2\alpha_o V_{ref}}{LC}(1 + u^{*2}) - \frac{2\alpha_o E}{LC} \\ + \frac{\alpha_o R_L}{LC}\frac{V_{ref}}{R} &+ \alpha_o u^*\frac{(4V_{ref} - 2E_o)}{L_oC_o} - \alpha_o u^*\frac{(4V_{ref} - 2E)}{LC}\end{aligned} \tag{36}$$

and is the solution to the following quadratic equation:

$$au^{*2} + bu^* + c = 0 \tag{37}$$

where

$$\begin{aligned} a &= 2\alpha_o V_{ref} \\ b &= -LC + \alpha_o(4V_{ref} - 2E_o)\frac{LC}{L_oC_o} - \alpha_o(4V_{ref} - 2E) \\ c &= 2\alpha_o V_{ref} - 2\alpha_o E + \alpha_o\frac{R_L}{R}V_{ref}\end{aligned} \tag{38}$$

whose feasible solution is

$$u^* = \frac{-b - \sqrt{(b^2 - 4ac)}}{2a} \tag{39}$$

The steady-state inductor current i_L^* is given by

$$i_L^* = \frac{V_{ref}}{(1 - u^*)R} \tag{40}$$

Remark 3: Let the $\tau_o = R_oC_0$ be the nominal time constant of the open-loop system with a decay constant $a_o = \tau_o^{-1}$. In view of (15) and (31), a possible general guideline for the choice of the controller and estimator gains is:

1) Choose $K_4 = 1$.
2) Choose $K_1 = ma_o$, with $m \geq 1$.
3) Choose $\gamma = K_1 + 100a_o$.
4) Choose $K_3 = \frac{K_1^2}{4}$.
5) Choose $K_2 = \frac{K_3}{10}$
6) If the performance is not adequate, increase m in step 2 and repeat.

III. Simulation Results

A. *Case 1: start-up transient with nominal parameters.*

The first simulation considers a start-up transient with $V_{ref} = 100\ V$ and using the nominal parameters listed in Table 1 for the implementation of the proposed sliding mode controller. The simulation is performed using the sampled model with a switching frequency $f_s = 100$ kHz. We also assume that $R_{L_1} = R_{L_2} = 0.1\ \Omega$ in the sampled model.

Using Remark 3 as a general guideline, the gains of the estimator/controller parameters are chosen as

$$\begin{gathered} K_1 = 2.5 \times 10^3,\ \gamma = 27.5 \times 10^3,\ K_2 = 156.250 \times 10^3, \\ K_3 = 1.5625 \times 10^6,\ K_4 = 1\end{gathered} \tag{41}$$

TABLE I
CONVERTER NOMINAL PARAMETERS

Nominal Parameters	Values and Units
Voltage supply	$E = 50$ V
Capacitor	$C = 200$ μF
Converter inductance	$L_1 = 76$ μH
Converter inductance	$L_2 = 76$ μH
Load resistance	$R = 20$ Ω

with $m = 10$ and the initial conditions of the state extended estimator $q_1(0) = 0,\ q_2(0) = 0$ and $q_3(0) = 0$.

Figure 2 shows the start-up transient output response reaching the reference voltage V_{ref} with no overshoot. Figure 3 depicts the current waveforms of the converter, and Figure 4 provides a magnified view showing the single-phase inductor ripple of 3.29 A and the input current ripple of 0.0658 A. This clearly demonstrates the benefit of the interleaved structure in reducing the input current ripple. Figure 5 shows the plot of the duty ratio u.

B. Case 2: start-up transient with uncertain parameters listed in Table 2 and parasitics given by (42).

In this case, we simulate the converter subjected to the parameter uncertainties listed in Table 2 along with the parasitics of the two parallel boost converters. Figure 6 shows the start-up transient output response reaching the reference voltage V_{ref} with no overshoot and tightly tracking the reference voltage V_{ref} with zero steady-state error. Figure 7 depicts the current waveforms of the converter, while Figure 8 provides a magnified view of Figure 7, showing a single-phase inductor ripple of 2.70 A and an input current ripple of 0.80 A. Please note that despite the converter operating in an unbalanced condition, there is only a small performance degradation, which is expected, in terms of a slight increase in the input current ripple and the output voltage ripple. Figure 9 shows the plot of the duty ratio u. We also assume the following parasitics in the sampled model:

TABLE II
CONVERTER PARAMETER UNCERTAINTIES

Nominal values	Actual values, increase/decrease
E=50 V	E=60 V **(+20 %)**
C=200 μF	C=140 μF $(\mathbf{-30}\%)$
$\mathrm{L}_1 = 76\ \mu H$	$\mathrm{L}_1 = 91.2\mu H$ $(\mathbf{+20}\%)$
$\mathrm{L}_2 = 76\ \mu H$	$\mathrm{L}_2 = 95.0\mu H$ $(\mathbf{+25}\%)$
R=20 Ω	R=26 Ω $(\mathbf{+30}\%)$

$$
\begin{gathered}
R_{L_1} = 0.2\Omega,\ R_{DS_1} = 0.02\ \Omega,\ V_{D_1} = 0.6\ V,\ R_{D_1} = 0.3\Omega \\
R_{L_2} = 0.3\Omega,\ R_{DS_2} = 0.04\ \Omega,\ V_{D_2} = 0.5\ V,\ R_{D_2} = 0.35\Omega \\
R_C = 0.01\Omega
\end{gathered}
\tag{42}
$$

where the unknown parameters R_{L_i}, $\mathrm{R}_{DS_i}, R_{D_i}, V_{D_i}, i = 1, 2$ and R_C represent the inductor equivalent series resistance, the MOSFET on-resistance, the diode forward resistance, the conducting voltage of the diode and the capacitor equivalent series resistance, respectively of the two parallel-connected boost converter stages.

C. Case 3: Robustness to step load resistance and input voltage changes

To test the robustness of the controller to step load resistance changes and step input voltage changes with uncertain parameters listed in Table 2 and parasitics given by (42), we assume that the converter is subjected to a step load resistance of $-10\ \Omega$ at t=0.2 s and 10 Ω at t=0.4 s from the actual value of R. The converter is also subjected to a step input voltage of $-10\ V$ at t=0.6 s and 10 V at t=0.8 s from the actual value of E. Fig. 10 depicts the time evolution of the output voltage v_c. As seen in this simulation, the proposed controller exhibits an excellent disturbance suppression capability during load resistance and input voltage changes with small overshoots, undershoots and short recovery times.

D. Case 4: Robustness to time-varying load resistance and input voltage changes

To test the robustness of the proposed controller to time-varying disturbances and parameter uncertainties, we assume that the converter is subjected simultaneously to parameter uncertainties listed in Table 2, to parasitics given in (42) and to time-varying input voltage E and time-varying load resistance R shown in Figure 11. Figure 12, shows the output response tracking the reference voltage with a small steady-state error of 321 mV, due to the time-varying external disturbances.

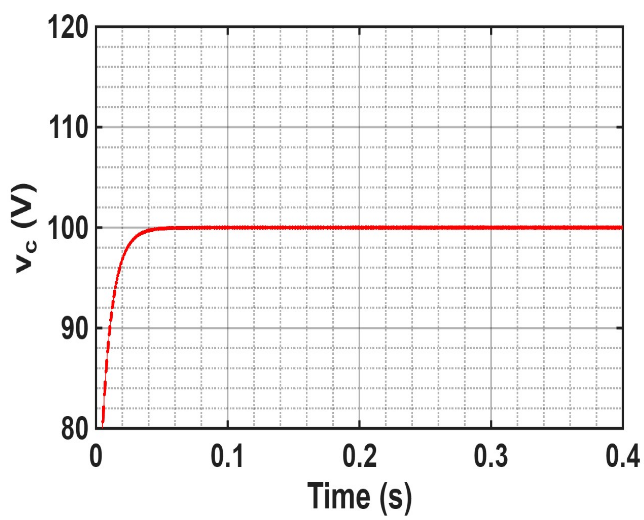

Fig. 2. Case 1: Output voltage Response using the nominal parameters listed in Table 1.

IV. CONCLUSION

This paper presents a PWM-based, current-sensorless robust sliding mode controller for the interleaved DC-DC boost converter, requiring only a single sensor for output voltage measurement. An extended state observer successfully estimates the derivative of the output voltage along with a lumped uncertainty signal that accounts for changing load resistances and input voltages, parametric variations, and circuit parasitics. A linear sliding surface is used to derive the control law. The

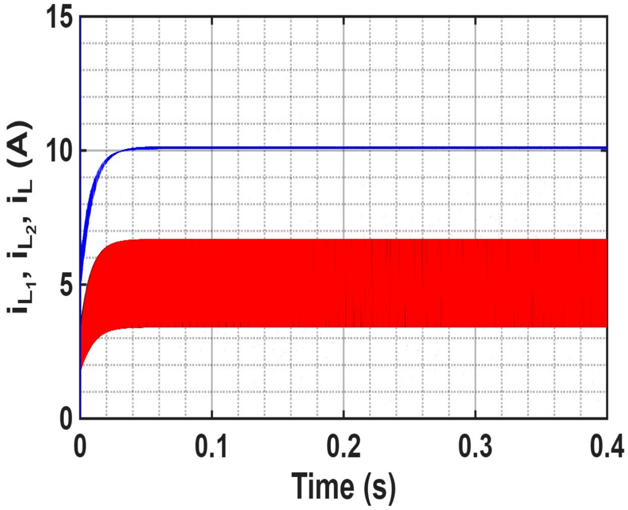

Fig. 3. Case 1: Inductor currents i_{L_1} in black, i_{L_2} in red, and i_L in blue.

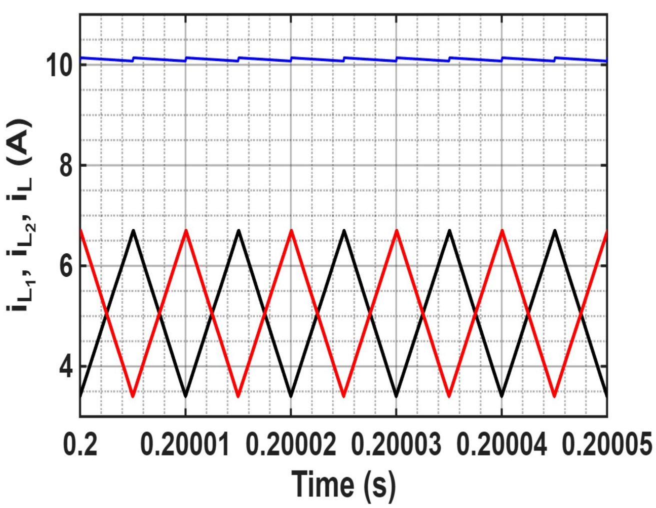

Fig. 4. Case 1: Zoom-in of Figure 3.

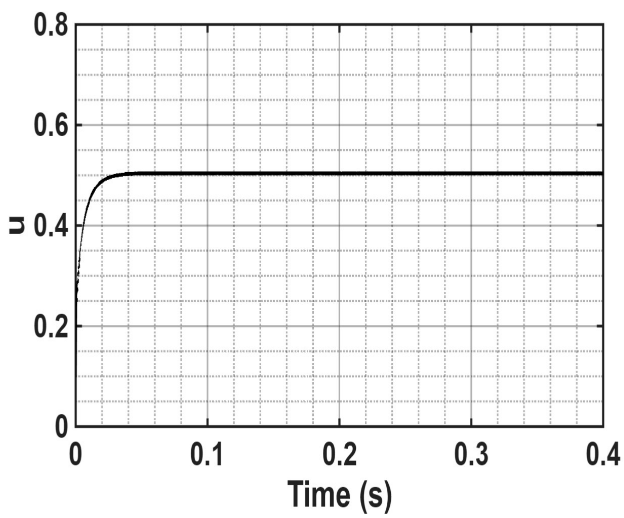

Fig. 5. Case 1: Duty ratio

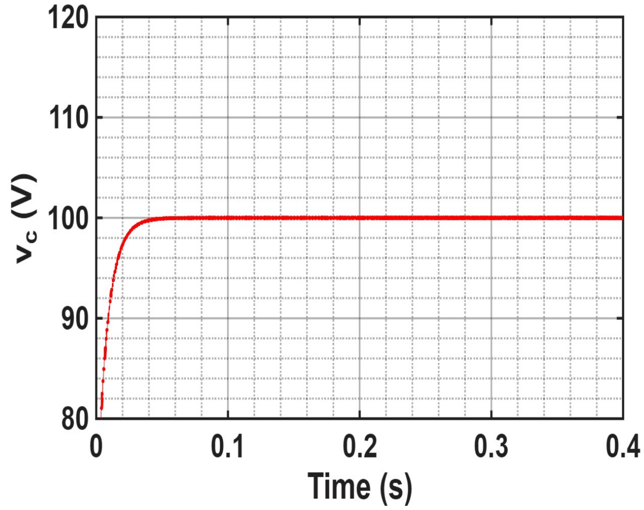

Fig. 6. Case 2: Output voltage response using the uncertain parameters listed in Table 2 and parasitics given by (42).

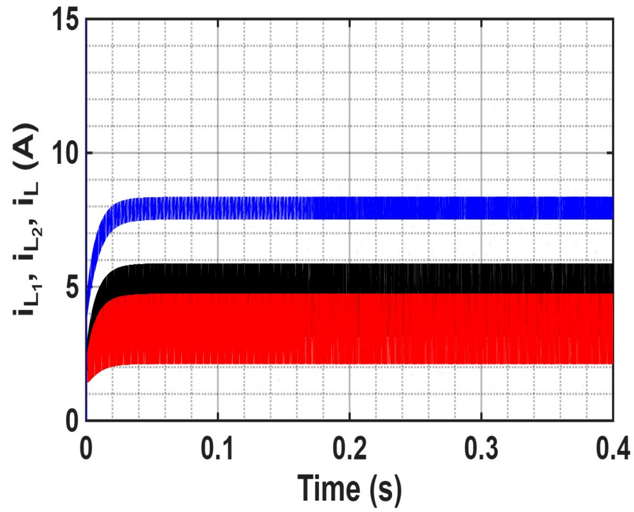

Fig. 7. Case 2: Inductor currents i_{L_1} in black, i_{L_2} in red, and i_L in blue.

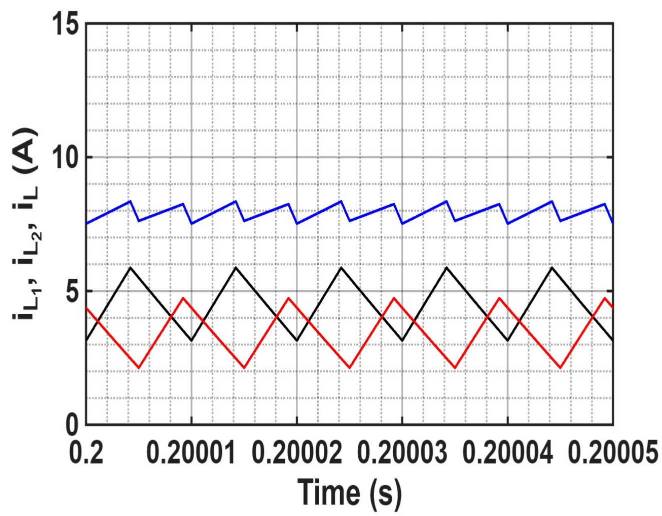

Fig. 8. Case 2: Zoom-in of Figure 7.

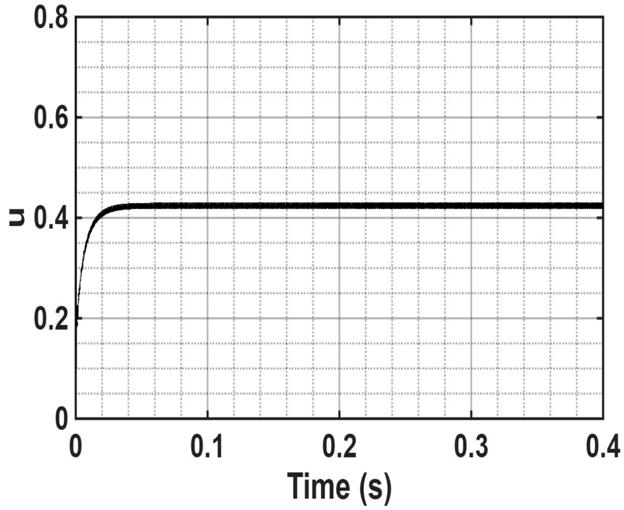

Fig. 9. Case 2: Duty ratio.

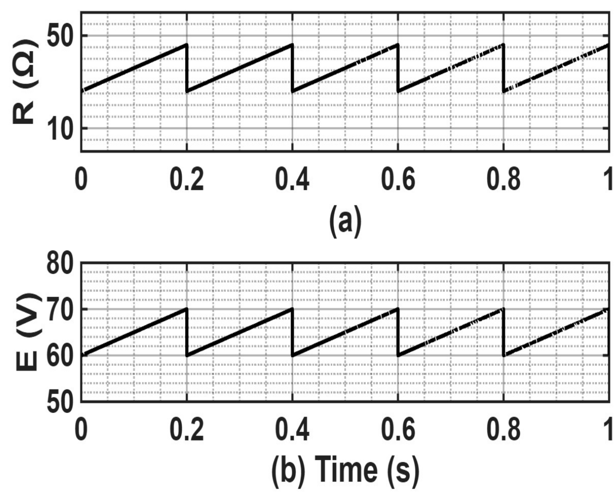

Fig. 11. Case 4: (a) Time-varying load resistance R and (b) time-varying input voltage E.

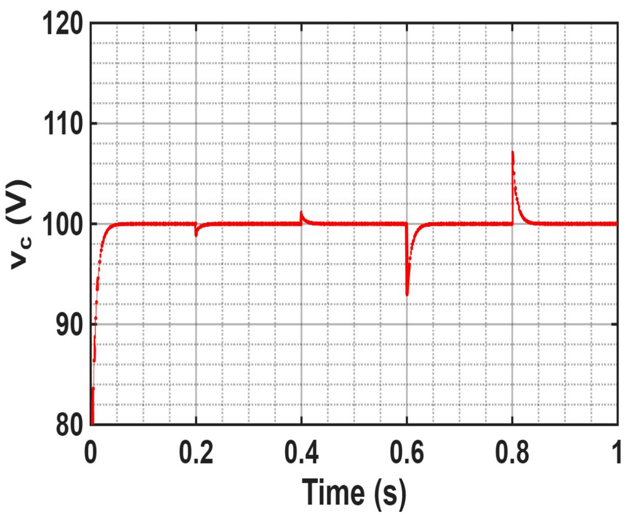

Fig. 10. Case 3: Output Response with step load resistance and input voltage changes with actual parameter of Table 2 and parasitics given by (42).

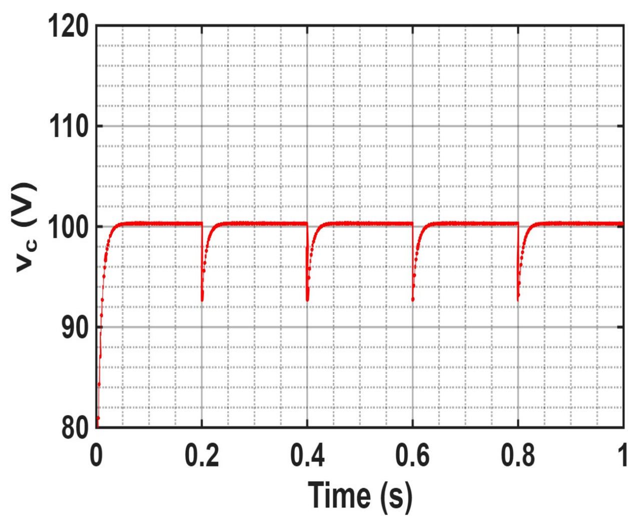

Fig. 12. Case 4: Output Response with time-varying input voltage and load resistance shown in Figure 11 with actual parameter of Table 2 and parasitics given by (42).

proposed controller features a simple design with a simple parameter-tuning procedure. Simulation results validate that the system achieves excellent disturbance suppression and dynamic compensation capabilities despite the complete absence of inductor current feedback. Future work will focus on the experimental validation of these theoretical and simulation results.

CONFLICT OF INTEREST

The authors declare that there is no competing financial interest that could have appeared to influence the work reported in this paper.

REFERENCES

[1] G. Cimini, G. Ippoliti, G. Orlando, S. Longhi, and R. Miceli, ”A unified observer for robust sensorless control of DC-DC converters,” Control Eng. Pract., vol. 61, pp. 21-27, Apr. 2017, doi: 10.1016/j.conengprac.2017.01.012.

[2] S. K. Pandey, S. L. Patil, U. M. Chaskar, and S. B. Phadke, ”State and disturbance observer-based integral sliding mode controlled boost DC-DC converters,” IEEE Trans. Circuits Syst. II, Exp. Briefs, vol. 66, no. 9, pp. 1567-1571, Sept. 2019, doi: 10.1109/TCSII.2018.2888570.

[3] M. Malekzadeh, A. Khosravi, and M. Tavan, ”A novel sensorless control scheme for DC-DC boost converter with global exponential stability,” Eur. Phys. J. Plus, vol. 134, no. 7, Art. no. 358, 2019, doi: 10.1140/epjp/i2019-12664-4.

[4] M. Malekzadeh, A. Khosravi, and M. Tavan, ”A novel adaptive output feedback control for DC-DC boost converter using immersion and invariance observer,” Evol. Syst., vol. 11, no. 4, pp. 707-715, 2020, doi: 10.1007/s12530-019-09268-7.

[5] X. Zhang, M. Martinez-Lopez, W. He, Y. Shang, C. Jiang, and J. Moreno-Valenzuela, ”Sensorless control for DC-DC boost converter via generalized parameter estimation-based observer,” Appl. Sci., vol. 11, no. 16, Art. no. 7761, 2021, doi: 10.3940/2076-3417/11/16/7761.

[6] S.-K. Kim and K.-B. Lee, ”Current-sensorless energy-shaping output voltage-tracking control for DC-DC boost converters with damping adaptation mechanism,” IEEE Trans. Power Electron., vol. 37, no. 8, pp. 9266-9274, Aug. 2022, doi: 10.1109/TPEL.2022.3159793.

[7] S.-K. Kim, C. Xu, and C. K. Ahn, ”Second-order disturbance-observer-based output-feedback voltage control of DC/DC converters

using pole-zero cancellation," IEEE Trans. Ind. Electron., vol. 73, no. 9, pp. 12905-12917, 2026, doi: 10.1109/TIE.2026.3677705.
[8] S. Oucheriah and A. Azad, "Current-sensorless robust sliding mode control for the DC-DC boost converter," AIMS Electron. Electr. Eng., vol. 9, no. 1, pp. 46-59, 2025, doi: 10.3934/electreng.2025003.
[9] W. Jiang, X. Zhang, F. Guo, J. Chen, P. Wang, and L. H. Koh, "Large-signal stability of interleave boost converter system with constant power load using sliding-mode control," IEEE Trans. Ind. Electron., vol. 67, no. 11, pp. 9450-9459, Nov. 2020, doi: 10.1109/TIE.2019.2955401.
[10] S. Zhuo et al., "Robust adaptive control of interleaved boost converter for fuel cell application," IEEE Trans. Ind. Appl., vol. 57, no. 6, pp. 6603-6610, Nov./Dec. 2021, doi: 10.1109/TIA.2021.3113262.
[11] H. Sartipizadeh, F. Harirchi, M. Babakmehr, and P. Dehghanian, "Robust model predictive control of DC-DC floating interleaved boost converter with multiple uncertainties," IEEE Trans. Energy Convers., vol. 36, no. 2, pp. 1403-1412, June 2021, doi: 10.1109/TEC.2021.3058524.
[12] J. Wachter, L. Grll, and V. Hagenmeyer, "Experimental analysis of immersion and invariance adaptive control for an interleaved DC/DC boost converter with unknown load type," in Proc. IEEE PES Innov. Smart Grid Technol. Eur. (ISGT EUROPE), Grenoble, France, 2023, pp. 1-6, doi: 10.1109/ISGTEUROPE56780.2023.10407194.
[13] Z. Dai, J. Liu, K. Li, Z. Mai, and G. Xue, "Research on a modeling and control strategy for interleaved boost converters with coupled inductors," Energies, vol. 16, no. 9, Art. no. 3810, 2023, doi: 10.3390/en16093810.
[14] A. Sferlazza et al., "Robust disturbance rejection control of DC/DC interleaved boost converters with additional sliding mode component," in Proc. Asia Meet. Environ. Electr. Eng. (EEE-AM), Hanoi, Vietnam, 2023, pp. 1-6, doi: 10.1109/EEEAM58328.2023.10395325.
[15] S. V. Malge et al., "Inductor current estimation based sensorless control of boost type DC-DC converter," Control Eng. Pract., vol. 153, Art. no. 106119, 2024, doi: 10.1016/j.conengprac.2024.106119.
[16] A. Mishra et al., "Non-linear control of interleaved boost converter using disturbance observer-based approach," IEEE Access, vol. 13, pp. 23833-23840, 2025, doi: 10.1109/ACCESS.2025.3537826.
[17] G. Garraffa et al., "Robust control of interleaved boost converter with active disturbance compensation," Control Eng. Pract., vol. 169, Art. no. 106746, 2026, doi: 10.1016/j.conengprac.2025.106746.